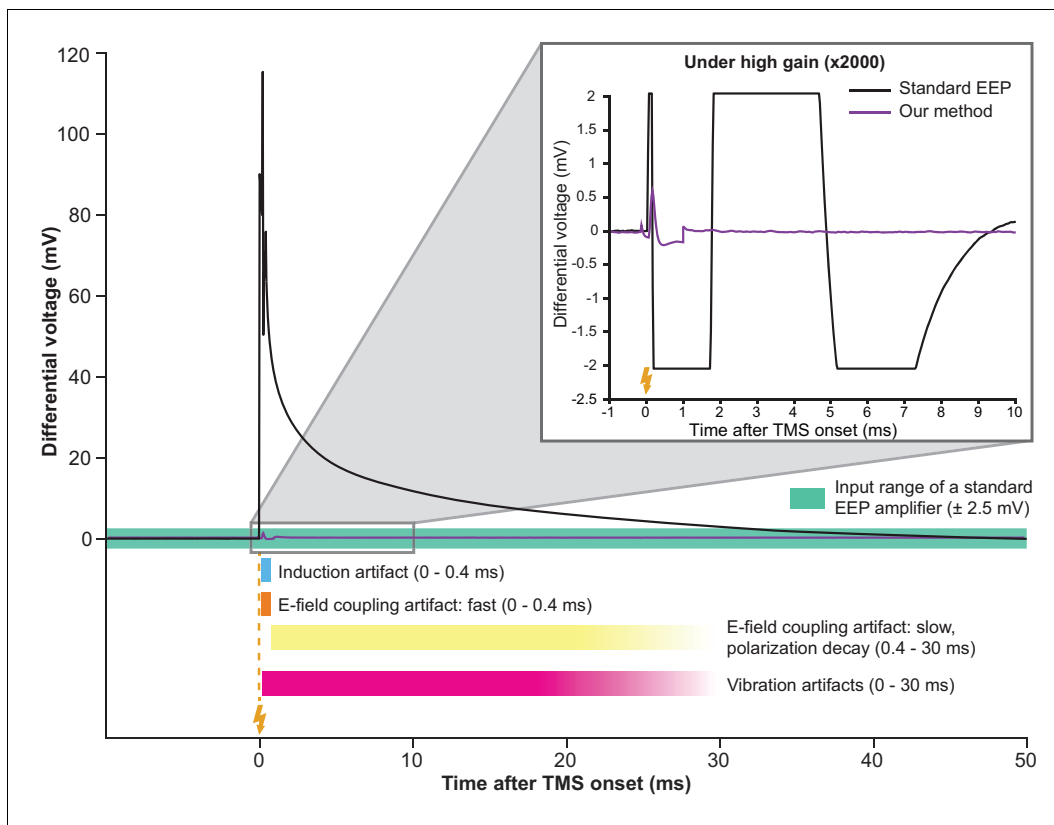


---

## Figures and figure supplements

Lifting the veil on the dynamics of neuronal activities evoked by transcranial magnetic stimulation

**Bingshuo Li *et al***



**Figure 1.** Simultaneous TMS-EEP recording requires artifact attenuation in multiple dimensions. The full waveform of a TMS artifact recorded differentially under low-gain (x4) using a high impedance amplifier. The artifact consists of a series of sharp deflections (induction and fast E-field coupling artifacts) and a long tail (polarization decay artifact resulted from E-field coupling). The slow polarization decay artifact renders the signal out of range (indicated by the green area) until ca. 30 ms post-TMS in a standard EEP system. Vibration artifacts (see **Figure 4B**) are not visible here due to low amplification. The inset shows that under high-gain (x2000) needed for EEP, TMS artifacts lead to long signal saturation in a standard EEP system (bandpass 300–5000 Hz) while producing negligible interference in our method. Lightning symbol, TMS onset (at 0 ms). E-field, electric field.

DOI: <https://doi.org/10.7554/eLife.30552.003>

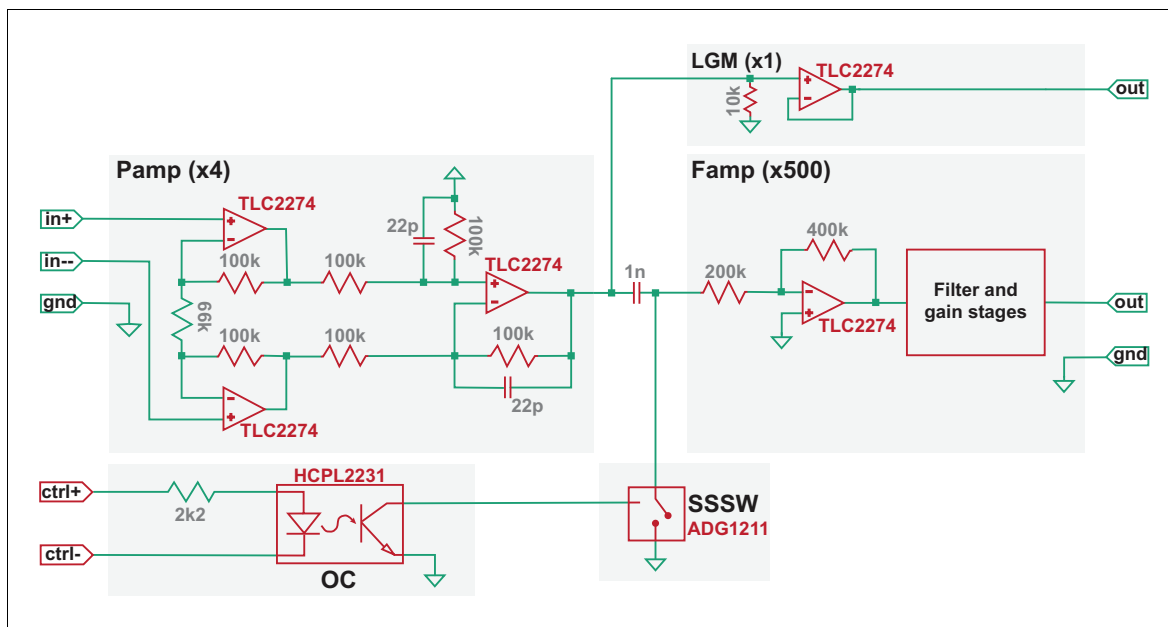


**Figure 2.** Simplified circuit diagram of the TMS-EEP amplifier. Model numbers of the most critical electronic components are noted in red, the values of certain elementary components are noted in grey (units: ohm for resistor; farad for capacitor), and the amplification factor for each stage is indicated in parenthesis. Pamp, pre-amplifier stage; Famp, filter-amplifier stage; OC, optocoupler; SSSW, solid-state analog switch; LGM, low-gain monitoring channel.

DOI: <https://doi.org/10.7554/eLife.30552.004>

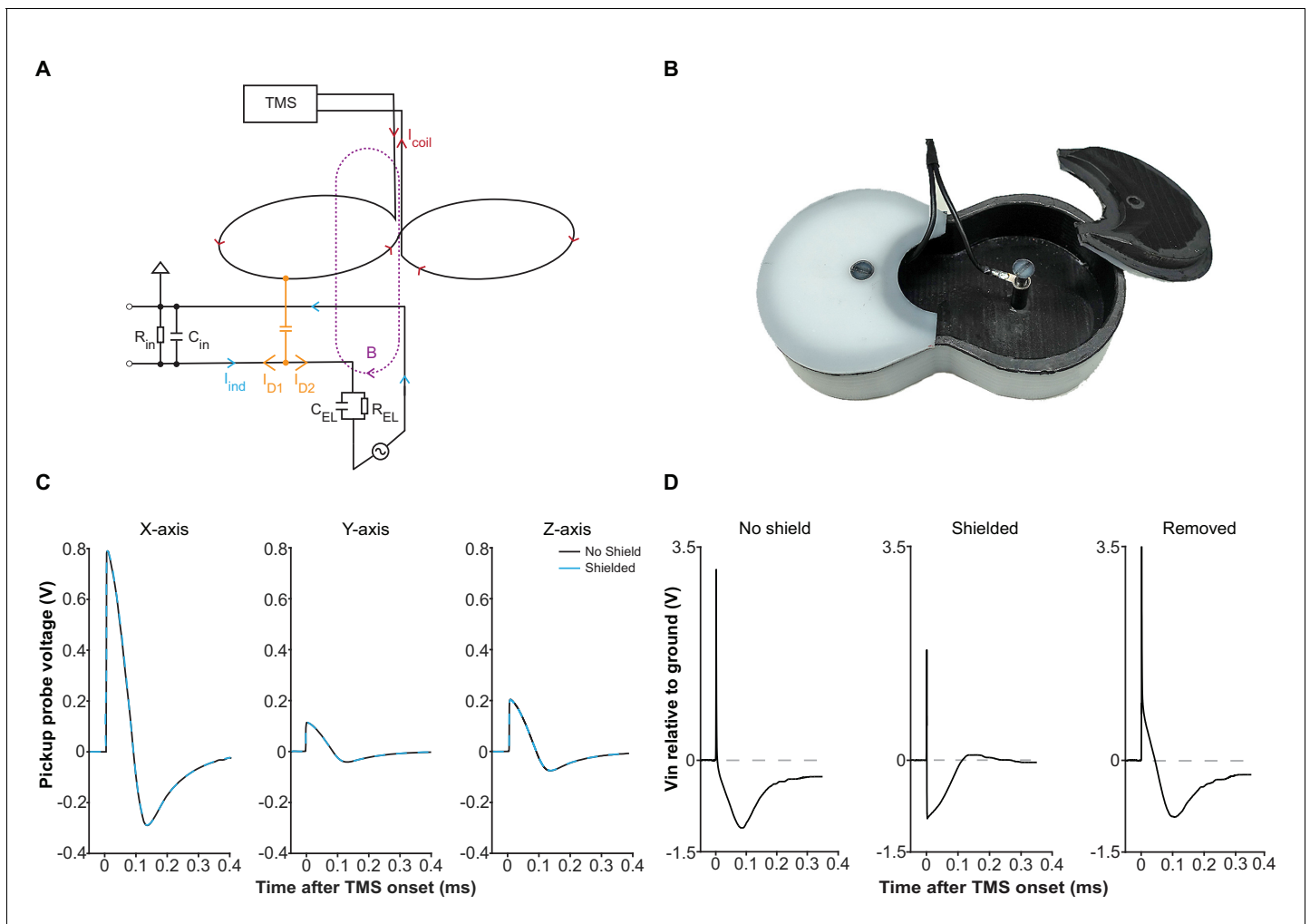


**Figure 3.** Electric field coupling in TMS-EEP and its attenuation. **(A)** A schematic illustrating how electric field coupling interferes with the EEP recording circuit. Here, the loop between one microelectrode and the ground is used as an example. The microelectrode is modeled as a parallel resistor-capacitor for simplification. Note how displacement current ( $I_D$ ), generated by electric field coupling, propagates in both directions once it enters the circuit, while the magnetically induced current ( $I_{ind}$ ) only propagates in a circular manner. The branch of displacement current ( $I_{D1}$ ) that flows toward the input end of the amplifier opposes the  $I_{ind}$ , counteracting the magnetically induced voltage change across the amplifier input resistance ( $R_{in}$ ). The other branch ( $I_{D2}$ ) flows toward the electrode and can cause polarization at the microelectrode tip. Abbreviations: B, magnetic field;  $C_{EL}$ , electrode capacitance;  $C_{in}$ , amplifier input capacitance;  $I_{coil}$ , TMS coil current;  $R_{EL}$ , electrode resistance. **(B)** The electrical shield constructed for the Magstim D25 coil. The shield fits tightly with the coil and is grounded through the EEP recording system. **(C)** Induction waveforms from a pickup probe positioned right below the coil center, along the X-, Y- and Z- axis, with or without the shield, under mspTMS at maximum intensity. Along each axis, the waveforms obtained under shielded and no shield condition overlap, confirming that the shield does not attenuate the magnetic output of the TMS coil. **(D)** Input voltage to a high impedance buffer (AD825,  $V_s = \pm 15V$ ), measured with a  $1.5 M\Omega$  (1 kHz) microelectrode, and an Ag/AgCl ground electrode in normal saline under mspTMS at maximum intensity with or without the shield. Signal in the 'Removed' condition was obtained by taking the difference between the waveforms in 'No shield' and 'Shielded' condition. The shield restored the correct induction waveform and abolished the voltage offset that leads to the decay.

DOI: <https://doi.org/10.7554/eLife.30552.005>

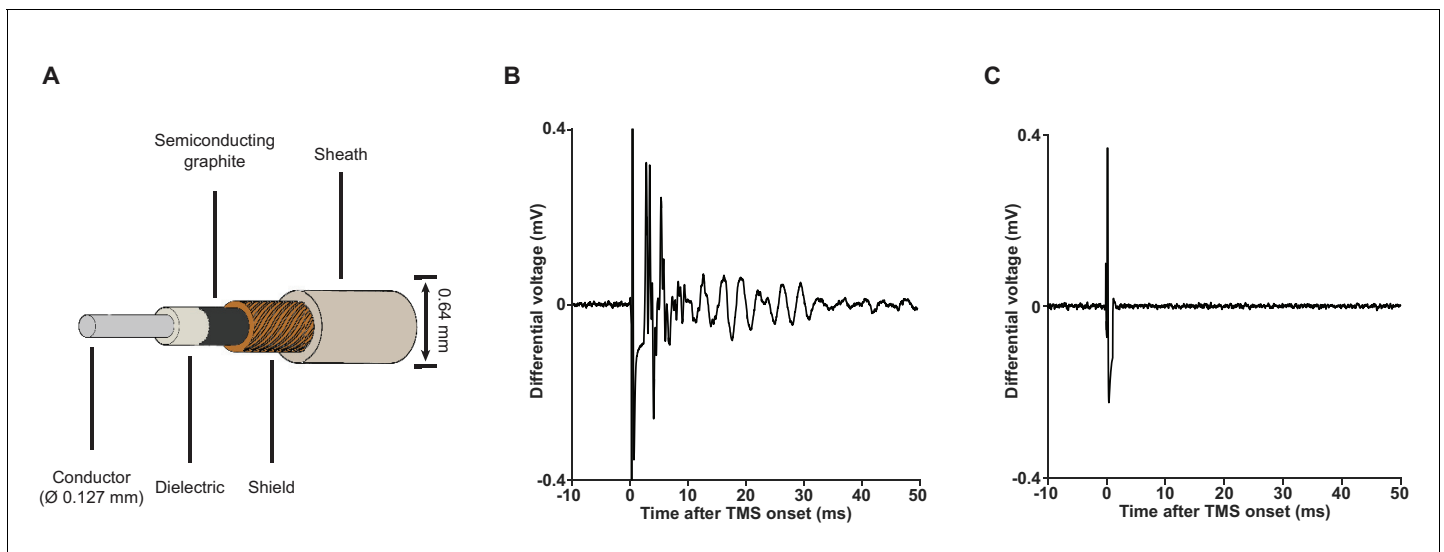


**Figure 4.** Low-noise miniature coaxial cable attenuates vibration artifacts. (A) A schematic illustration of the 36-gauge low-noise miniature coaxial cable. A semiconducting layer of graphite is added between the braided shield and the dielectric of the cable to drain triboelectric charges, rendering the cable insensitive to vibration. (B) An example of vibration artifacts recorded under the standard EEP conditions (x2000 using our TMS-EEP amplifier; 1.5 M $\Omega$  microelectrode pair; Ag/AgCl ground electrode; normal miniature coaxial cable) in a saline bath after induction and electric field coupling artifacts were suppressed. The vibration artifacts can manifest in multiple types of waveform, depending on the parts of the recording assembly that are perturbed and the resonance properties of these parts. (C) The implementation of low-noise miniature coaxial cables attenuated the vibrational artifacts. Signal recorded under conditions identical to those in (B) except the cables.

DOI: <https://doi.org/10.7554/eLife.30552.006>

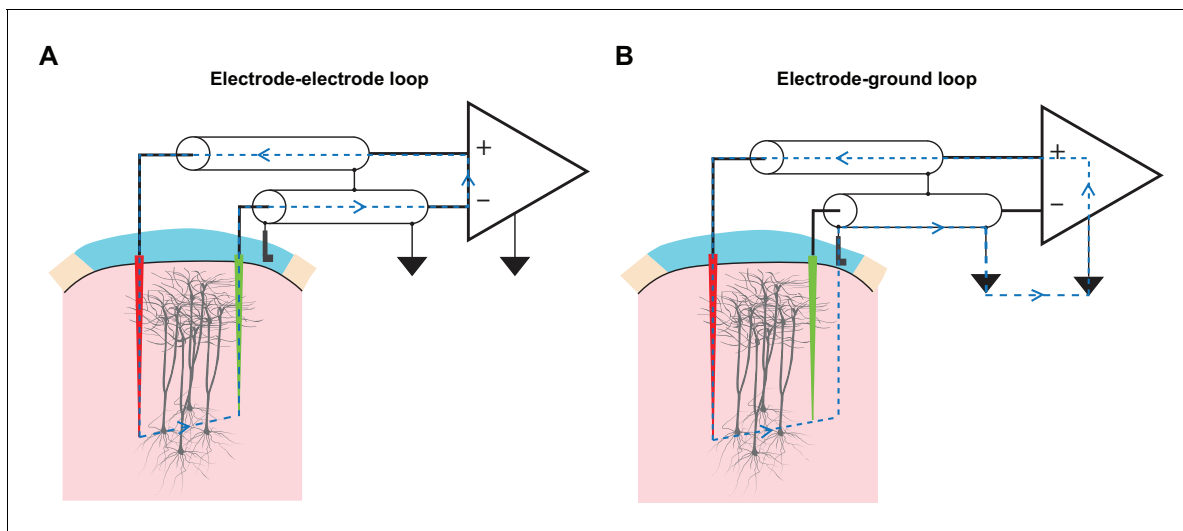


**Figure 5.** TMS drives inadvertent charge injection in multiple loops formed by an EEP recording assembly. **(A)** A schematic illustration of the induction loop formed between the recording (red) and the reference (green) microelectrode under TMS. In the case that TMS-induced voltage is high enough, a substantial amount of electrical current (blue dashed lines) can flow within the loop and subsequently, this may inadvertently stimulate neuronal elements around the microelectrode tips. **(B)** A schematic illustration of the induction loop formed between a microelectrode and the ground electrode under TMS.

DOI: <https://doi.org/10.7554/eLife.30552.007>

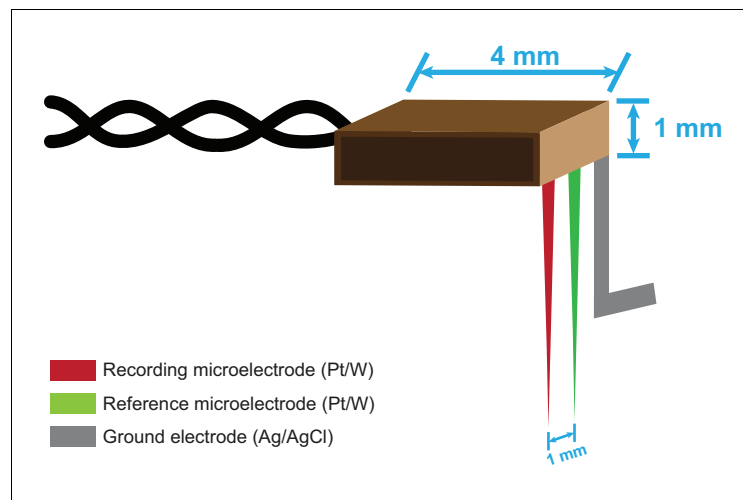


**Figure 5—figure supplement 1.** The three-pronged electrode set design. We fabricated in-house a three-pronged electrode set that minimizes the area of induction loops under TMS. The microelectrodes are connected to a pair of twisted low-noise miniature coaxial cables, and the ground electrode is connected to the coaxial cable shield. A macroscopic view of the electrode set in a recording setup is shown in **Figure 6A**.

DOI: <https://doi.org/10.7554/eLife.30552.008>

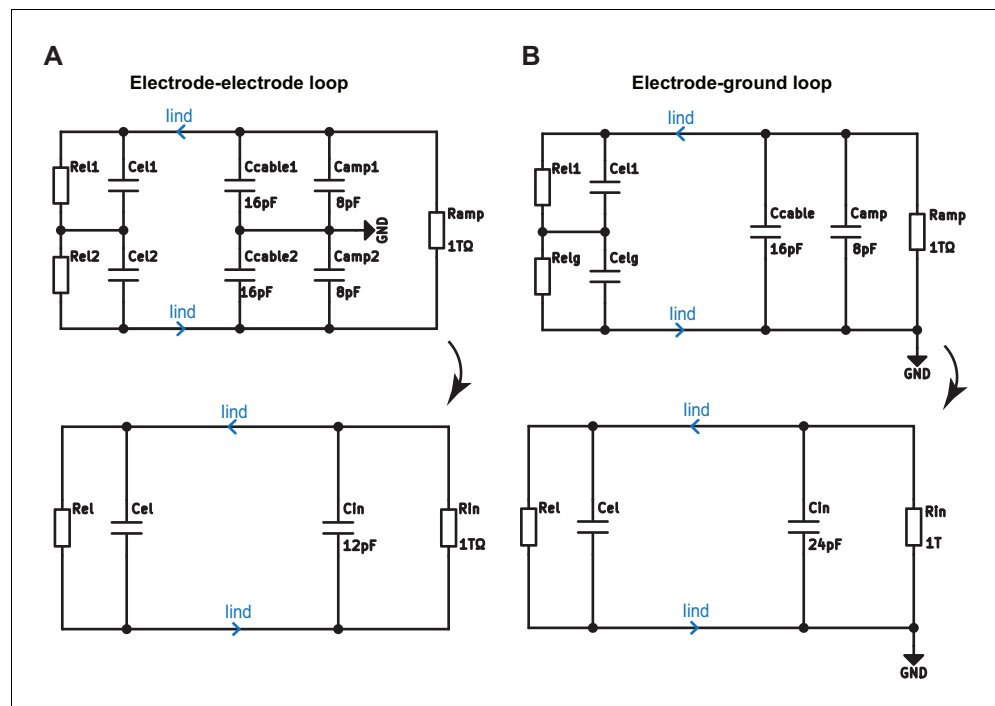


**Figure 5—figure supplement 2.** Circuit representations of the two induction loops shown in **Figure 5**. Circuit component abbreviations: amp, amplifier; C, capacitance; el1, recording microelectrode; el2, reference microelectrode; elg, ground electrode; GND, amplifier ground; in, input;  $I_{ind}$ , induction current; R, resistance.

DOI: <https://doi.org/10.7554/eLife.30552.009>



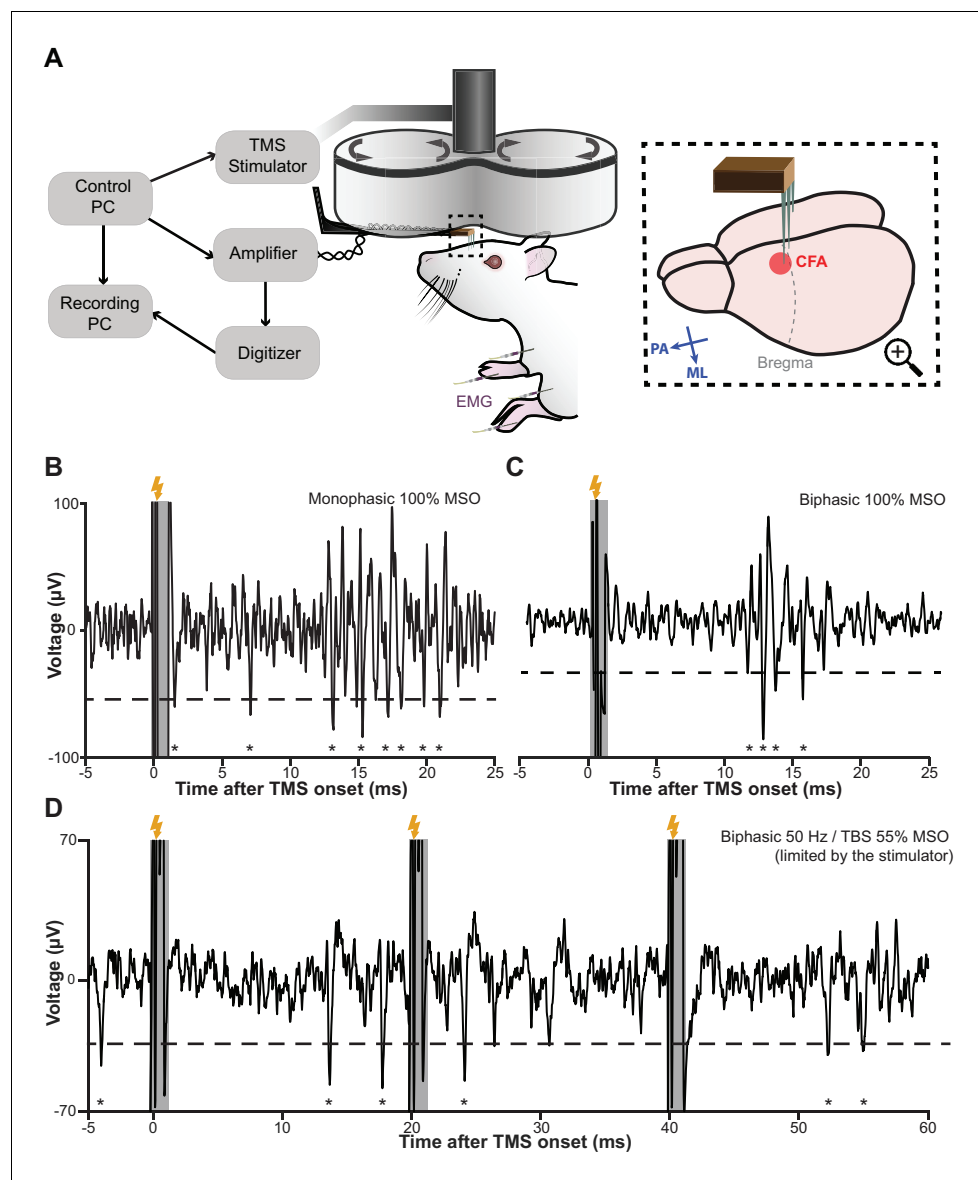


**Figure 6.** TMS-EEP recording setup and rapid signal recovery under the worst-case TMS stimuli. (A) A schematic illustration of our recording setup. Thick arrows, direction of coil current; inset blue arrows, direction of induced current in the brain; ML, medial-lateral; PA, posterior-anterior; CFA, caudal forelimb area (rodent's equivalent to forelimb M1 in primates); EMG, intramuscular electromyography. (B–D) A sample trace of in vivo recordings under the worst-possible (see Materials and methods) monophasic, biphasic, and theta-burst (first three pulses) stimulus, respectively. The short transient (–0.2 to +0.8 ms) during which the amplifier is protected from the induction artifact is indicated in gray. Lightning symbol, TMS onset (at 0 ms); dashed line, spike detection threshold (see Materials and methods); asterisks, extracellular spikes.

DOI: <https://doi.org/10.7554/eLife.30552.010>

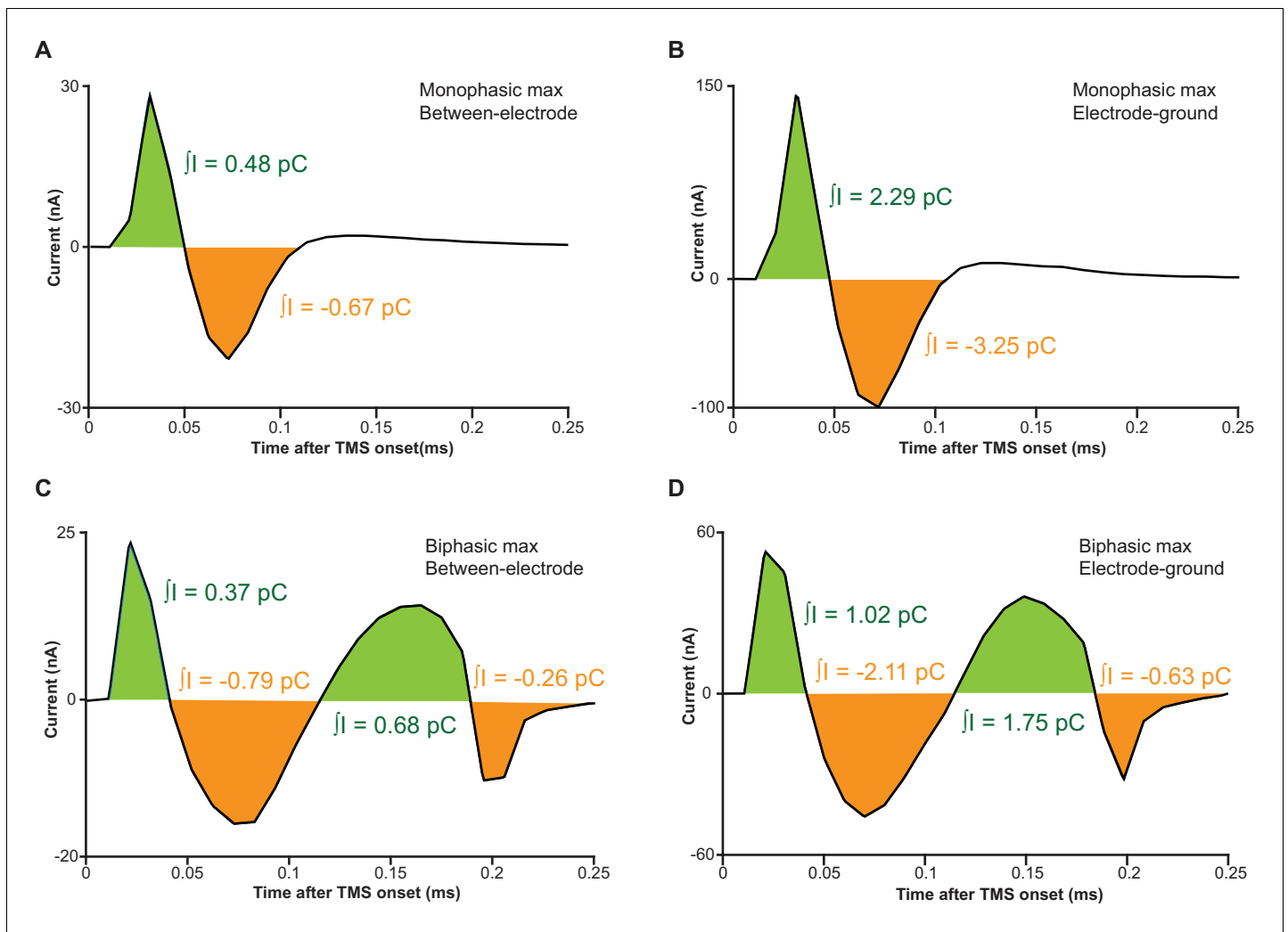


**Figure 6—figure supplement 1.** In vivo measurements of inadvertent charge injection. Under the worst-possible stimuli (see Materials and methods), the in vivo measured values of induction current (y-axis) and charge transfer (integral of y) are shown. All values obtained are far below (by a factor of 200 or more) the modulation and the activation thresholds reported in the ICMS literature (*Asanuma and Rosén, 1973; Butovas and Schwarz, 2003*). Therefore, it can be concluded that under our recording setup, neurobiological effects of inadvertent charge injection can be neglected.

DOI: <https://doi.org/10.7554/eLife.30552.011>

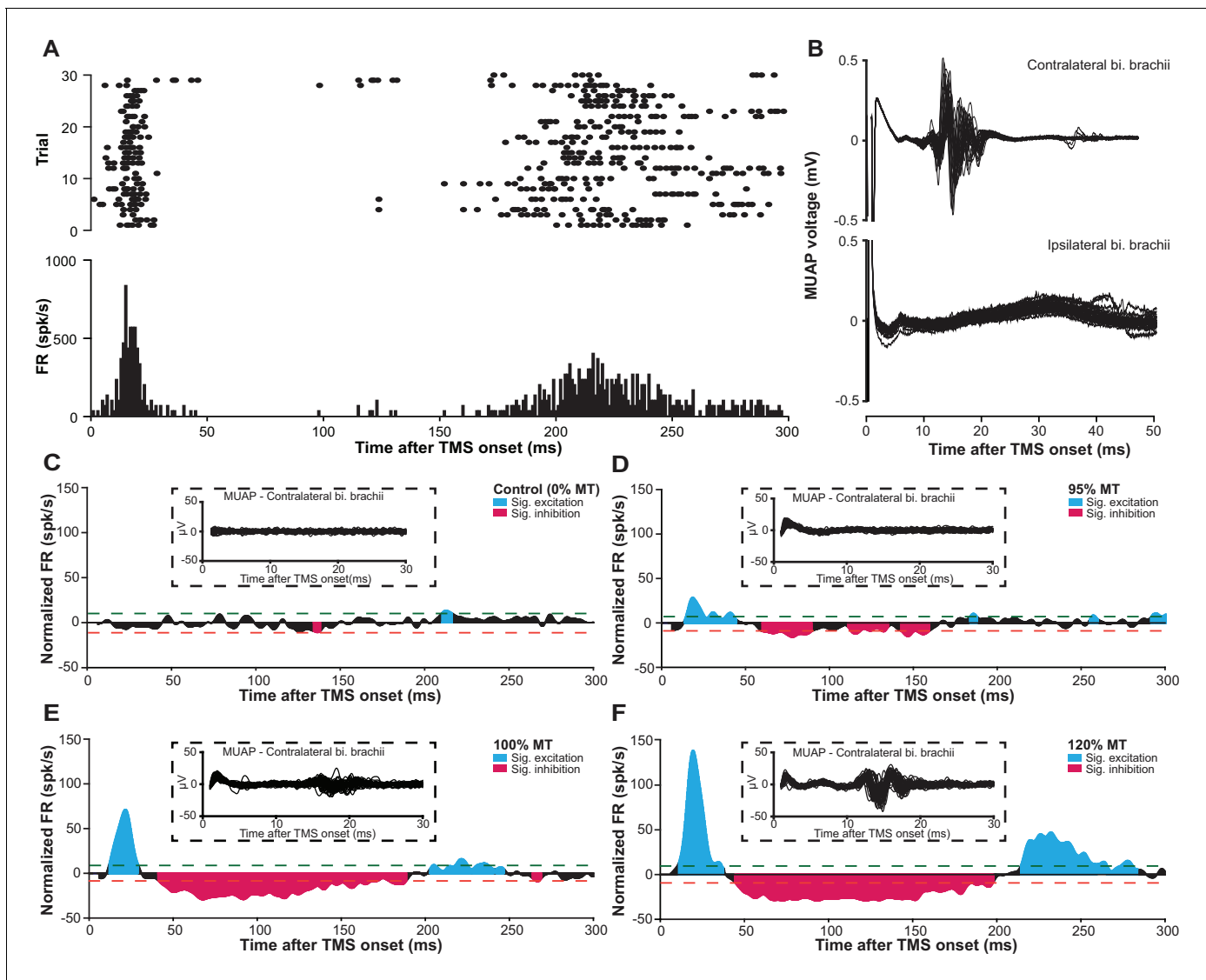


**Figure 7.** mspTMS evoked multiphasic response alternating between excitation and inhibition. (A) Raster plot (top) and PSTH (bottom; binsize 1 ms) of multiunit spike activity evoked by mspTMS (stimulus orientation ML; intensity 120% MT; onset at 0 ms) recorded in layer V of the CFA from one animal. (B) Traces of evoked MUAPs (corresponding to trials in A) obtained by intramuscular EMG in the biceps (bi.) brachii muscle contralateral and ipsilateral to the stimulated CFA. (C–F) Population average (N = 7) of normalized multiunit FR in the layer V of CFA evoked by ML-oriented mspTMS of increasing intensity. The PSTHs were smoothed by a Gaussian kernel for visualization. Inset, example traces of evoked MUAP in the contralateral bi. brachii from one animal. Dashed lines, significance thresholds determined by the 2.5 or 97.5 percentile of the empirical distribution of baseline normalized FR (see Materials and methods for details).

DOI: <https://doi.org/10.7554/eLife.30552.012>

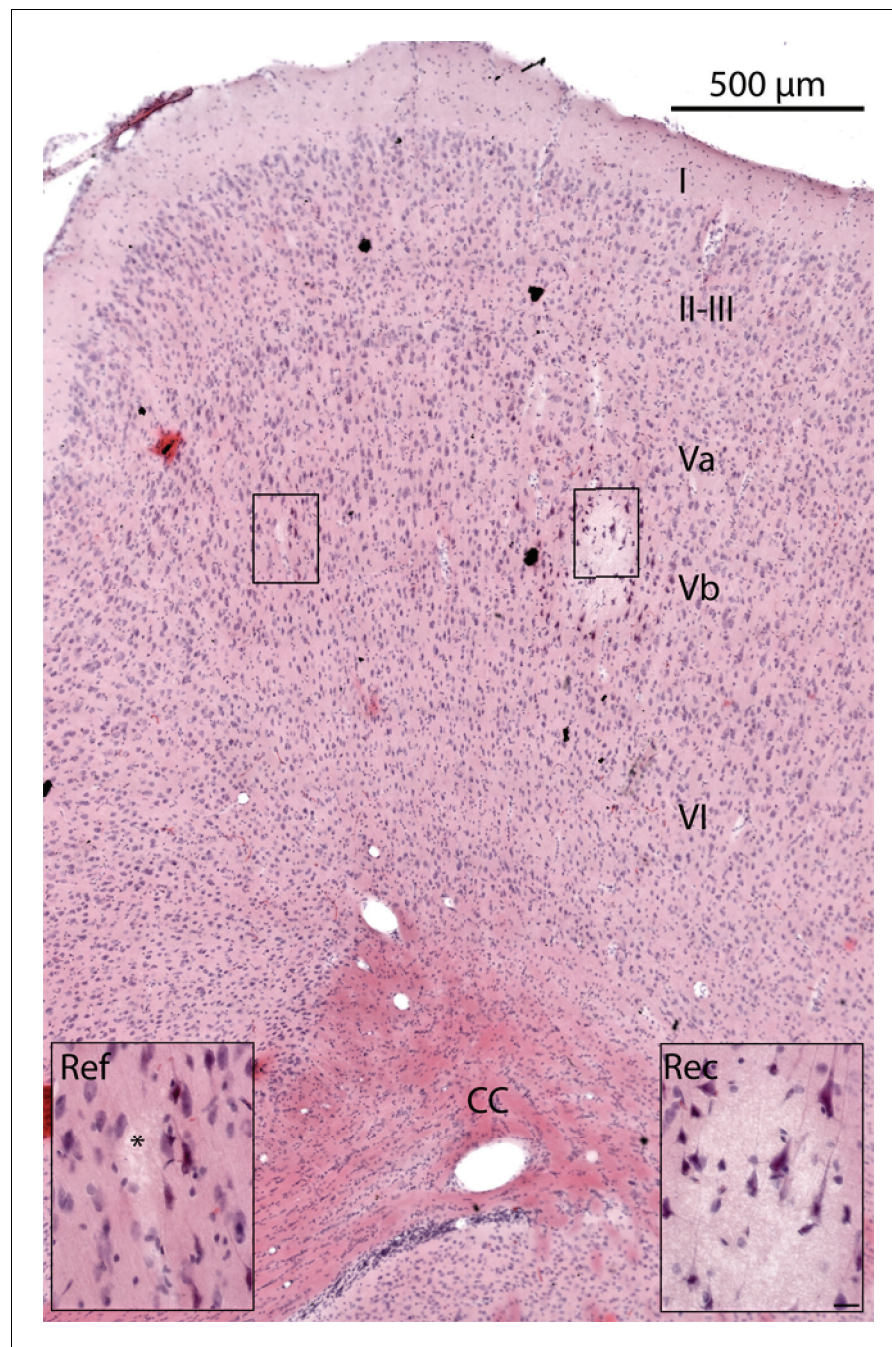


**Figure 7—figure supplement 1.** Histological confirmation of electrode placement. The hematoxylin and eosin stained coronal section confirms the placement of recording electrode (Rec) in layer Vb of CFA and the placement of reference electrode (Ref) outside of the primary motor cortex. The location of Rec was marked by an electrolytic lesion after the experiment and the location of Ref, while not marked by lesioning, is also visible (\* in the left inset). The scale bar for the insets represents 20  $\mu$ m distance. CC indicates corpus callosum. Latin numbers I to VI represent the different cortical layers.

DOI: <https://doi.org/10.7554/eLife.30552.013>

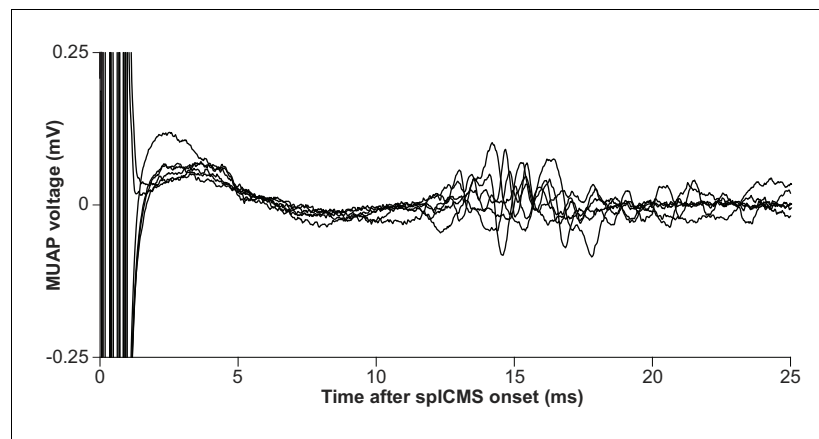


**Figure 7—figure supplement 2.** MUAP evoked by single-pulse ICMS. In one animal, we stimulated layer V of the left CFA with a single ICMS pulse and recorded intramuscular EMG in both left (ipsilateral to the stimulated motor cortex; not shown) and right (contralateral) biceps brachii. The evoked MUAPs, detected solely in the right biceps brachii, displayed onset latencies (11–12 ms) similar to those obtained in our TMS experiment, suggesting the cortical origin of the TMS-evoked MUAPs.

DOI: <https://doi.org/10.7554/eLife.30552.014>

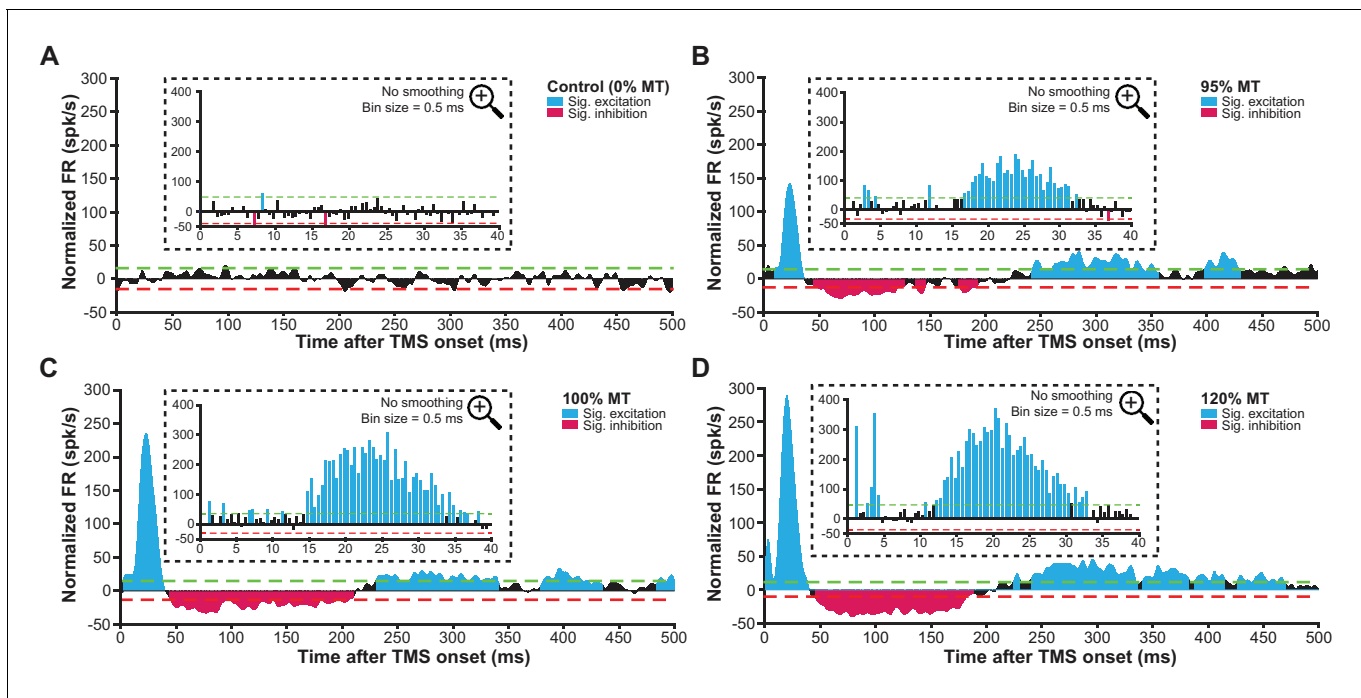


**Figure 7—figure supplement 3.** Layer V neuronal response evoked by PA-oriented mspTMS at different intensities. Population average ( $N = 4$ ) of normalized multiunit FR in layer V of CFA evoked by PA-oriented mspTMS. The histograms were constructed using the same procedures as those described for **Figure 7C–F**. Insets, zoom-ins (0–40 ms) on the PSTH of evoked normalized FR with no smoothing. Dashed lines, significance thresholds determined by the 2.5 or 97.5 percentile of the empirical distribution of baseline normalized FR (see Materials and methods for details). TMS was delivered at time 0 ms.

DOI: <https://doi.org/10.7554/eLife.30552.015>

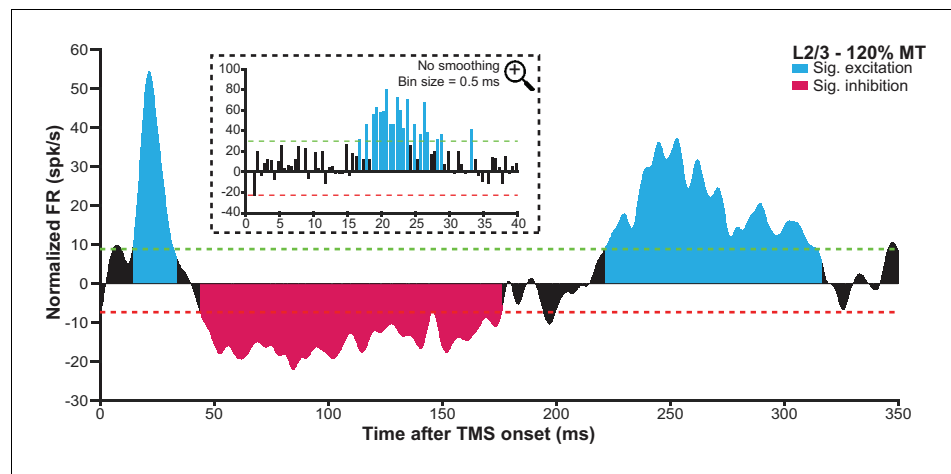


**Figure 7—figure supplement 4.** mspTMS evoked a multiphasic pattern of neuronal response in layer II/III. In five animals (299 trials total), we recorded multiunit activities in layer II/III (400  $\mu$ m from the cortical surface) of the CFA under mspTMS (ML orientation) at 120% MT. The histograms were constructed using the same procedures as those described for **Figure 7C–F**. The TMS-evoked multiphasic pattern of FR found here is qualitatively similar to that obtained in layer V (**Figure 7C–F**). Insets, zoom-ins (0–40 ms) on the PSTH of evoked normalized FR with no smoothing. Dashed lines, significance thresholds determined by the 2.5 or 97.5 percentile of the empirical distribution of baseline normalized FR (see Materials and methods for details). TMS was delivered at time 0 ms. DOI: <https://doi.org/10.7554/eLife.30552.016>

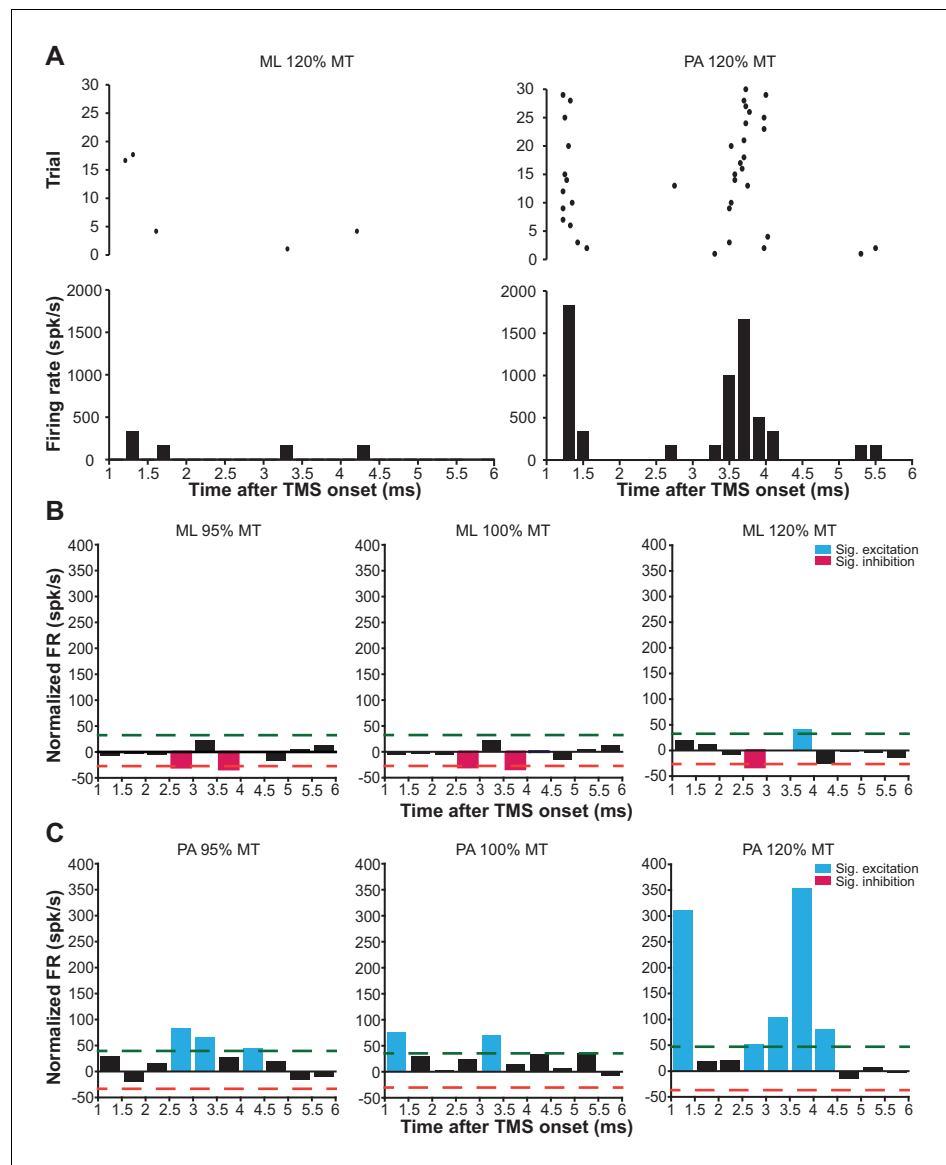


**Figure 8.** mspTMS-evoked short-latency neuronal responses differ with stimulus orientations. (A) Examples of short-latency (1–6 ms) multiunit response in layer V of the CFA to suprathreshold mspTMS (120% MT) oriented in ML and PA direction. The suprathreshold ML stimulus evoked virtually no response in this time window, whereas the PA stimulus evoked strong periodic firing in the neuronal population. Note, all orientations discussed here refer to the orientation of induced current in the brain. (B–C) Average of short-latency normalized multiunit FR (binsize 0.5 ms) across all animals tested with the ML- (B) and PA- (C) oriented mspTMS at increasing intensities. Dashed lines, significance thresholds determined by the 2.5 or 97.5 percentile of the empirical distribution of baseline normalized multiunit FR (see Materials and methods for details).

DOI: <https://doi.org/10.7554/eLife.30552.017>



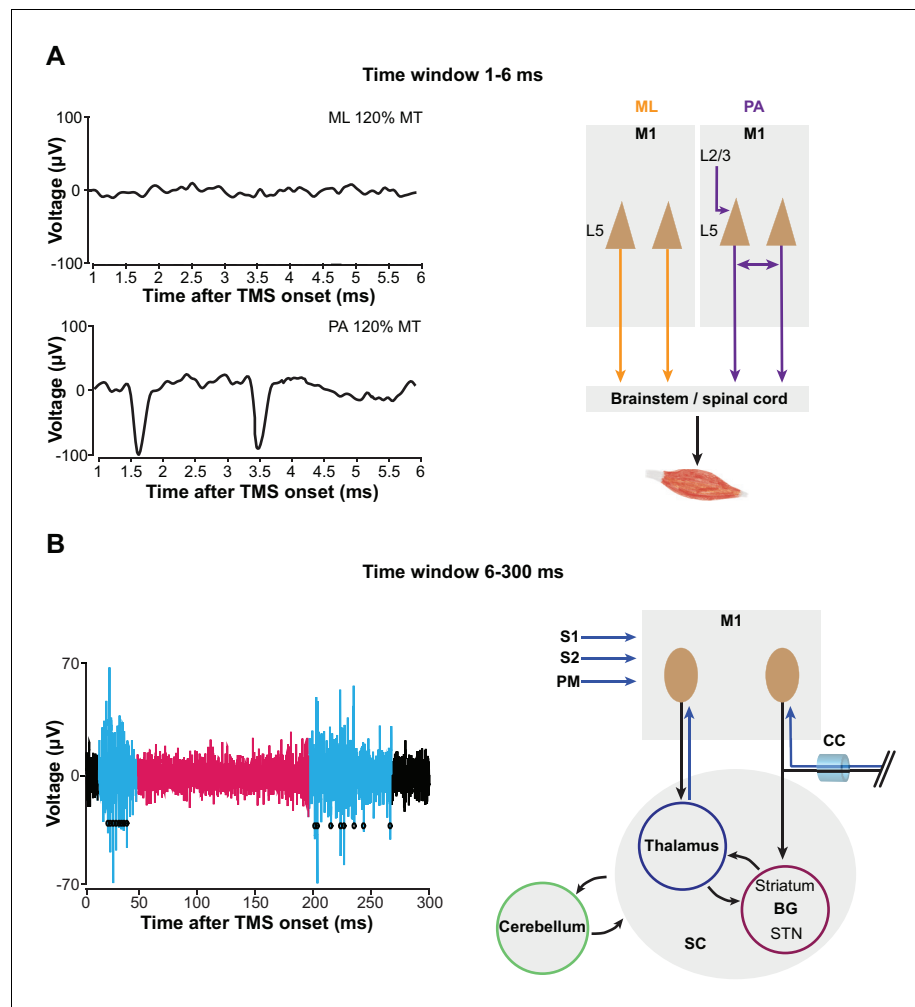


**Figure 9.** mspTMS activates different neuronal circuits depending on stimulus orientation or the time-window of investigation. (A) In the short-latency time window (1–6 ms after onset), ML- and PA-oriented mspTMS evoked different patterns of neuronal activities in layer V of CFA (left panel). ML stimuli activated the descending PT pathways, while PA stimuli triggered an oscillatory spiking event that reflects the local connectivity within M1 (right panel). (B) In the long-latency time window (6–300 ms after onset), mspTMS evoked a multiphasic response alternating between excitation and inhibition (left panel shows a raw spike trace evoked by a suprathreshold stimulus; blue and red code for phase of significant excitation and inhibition, respectively, adopted from **Figure 7**). This multiphasic pattern is generated through multiple possible long-range circuits activated by mspTMS (right panel). Abbreviations: BG, basal ganglia; CC, corpus callosum; M1, primary motor cortex; PM, premotor cortex; S1/S2, somatosensory cortices; SC, subcortical structures; STN, subthalamic nucleus.

DOI: <https://doi.org/10.7554/eLife.30552.018>